Impurity studies for the ITER half-field ICRF heating scenarios in hydrogen plasmas on JET

Agata Czarnecka,
Ernesto Lerche,
Jef Ongena,
Dirk Van Eester,
Antonio C. A. Figueiredo,
Ivor H. Coffey,
Klaus-Dieter Zastrow
and *JET-EFDA contributors**

Abstract. Two ion cyclotron range of frequencies (ICRF) heating scenarios, proposed for the non-activated half-B_0 phase of ITER in hydrogen plasmas, were investigated on the JET tokamak. This paper we present a detailed study of the impurity content in plasma when the fundamental H and the 2nd harmonic ^{3}He ICRF heating scenarios are realized. The ICRF conditions for those heating scenarios on ITER – i.e. the frequency of 42 MHz for the fundamental H and 53 MHz for the 2nd harmonic ^{3}He heating, and the magnetic field $B_0 = 2.65$ T – were closely reproduced in dedicated experiments on JET. The impurity content of the plasma was determined by means of the spectroscopy in the VUV range. The release of C and Ni impurities during the ICRF heating is presented as a function of the total ICRF heating power supplied in those heating scenarios. The contribution of the Ni impurity to the effective charge of the plasma, Z_{eff}, and the plasma dilution are estimated. We find that for the ^{3}He ICRF heating scenario the impurity content and the plasma energy loss through radiation was higher than for the fundamental hydrogen heating scenario.

Key words: tokamak • impurities • ICRF heating • ITER scenario • VUV plasma spectroscopy

A. Czarnecka✉
Institute of Plasma Physics and Laser Microfusion,
Association EURATOM-IPPLM,
23 Hery Str., 01-497 Warsaw, Poland,
Tel.: +48 22 638 1005, Fax: +48 22 683 8605,
E-mail: agata.czarnecka@ipplm.pl

E. Lerche, J. Ongena, D. Van Eester
Association "EURATOM – Belgian State",
ERM-KMS, TEC Partner,
30 de la Renaissance Ave., B-1000 Brussels, Belgium

A. C. A. Figueiredo
Associação Euratom/IST,
Instituto de Plasmas e Fusão Nuclear,
Instituto Superior Técnico,
Universidade Técnica de Lisboa,
1 Rovisco Pais Ave., 1049-001 Lisboa, Portugal

I. H. Coffey, K.-D. Zastrow
Euratom/CCFE Association,
Culham Science Centre,
Abingdon, OX14 3DB, UK

*See the Appendix of F. Romanelli *et al*., Fusion Energy Conference 2010 (Proc. 23nd Int. Conf. Daejeon, Korea, 2010. IAEA, Vienna 2010).

Introduction

Several modes of plasma operation and various ion cyclotron range of frequency (ICRF) heating scenarios are foreseen for ITER [6]. These include H, D, DT, and ^{4}He plasma operation. The initial, non-active phase of ITER [7] will start with hydrogen plasmas at half the nominal toroidal magnetic field $B_0 = 2.65$ T and the plasma current $I_p = 7.5$ MA [2]. The discharges are expected to be in the L-mode with a typical central density $n_e(0) \approx 3 \times 10^{19}$ m^{-3} and the central temperatures of approximately $T_i = 8$ keV and $T_e = 10$ keV [10]. The auxiliary heating systems foreseen for the initial phase are the neutral beam injection (NBI), the electron cyclotron range of frequency (ECRF) heating, and the ICRF heating. The ICRH antenna for ITER is expected to deliver 20 MW of heating power in the frequency range 40–55 MHz [13]. In this range there are limited possibilities to heat these plasmas by ICRH [11]. Two main candidate scenarios at half field are (a) N = 1 H at $f \approx 40$ MHz, and (b) the second harmonic ion cyclotron heating of ^{3}He ions (N = 2 ^{3}He) at $f \approx 53$ MHz. These two ICRF heating scenarios were closely reproduced in an experiment on JET [11]. However, the ICRF heating efficiency η (defined as the ratio of power transferred to the bulk plasma over the total coupled power) for these scenarios is rather low (η = 0.3–0.4) compared to typical heating efficiencies η > 0.8 of other minority ICRF heating schemes [10]. As a result, the waves of the heating radiation have to pass several times

through the plasma before being absorbed. This leads to a strong interaction of waves with the edge and an enhanced generation of impurities from the first wall. The aim of this work is to study the influence of the ITER half-field ICRF heating scenarios in H plasmas on the impurity behaviour in JET by means of VUV emission spectroscopy. Such a study is important to understand and minimize the effect of impurities on tokamak plasma performance.

Experimental setup

The ICRF heating parameters of the half-field phase of ITER were closely reproduced in experiments on JET. The fundamental hydrogen heating scenario and the N = 2 ^{3}He ICRF heating scenario were tested at frequencies of 42.5 MHz and 51.5 MHz, respectively. Under these conditions the fundamental ion cyclotron resonance layer of the H ions is located in JET around $R = 2.85$ m, whereas the N = 2 ion cyclotron resonance of the ^{3}He ions is located at approximately $R = 3.15$ m, as shown in Fig. 1. For the same conditions the fundamental ion cyclotron resonance layer of the H ions and the 2nd harmonic ion cyclotron resonance of the ^{3}He ions in ITER would be both located near the plasma centre, i.e. at $R = 6.2$ m. Experiments at JET were performed in the L-mode with the magnetic field $B_0 = 2.65$ T and the plasma current $I_p = 1.4$ MA. Both experiments adopted a plasma geometry that assures enhanced ICRF antenna coupling, with the distance between the antenna and the plasma varying in the range of 9.5–11.0 cm. The dipole phasing was used in all pulses. Up to 5.5 MW of ICRF power and up to 8 MW of NBI power were coupled to the plasma. Depending on the NBI power applied, typical central densities of $n_e(0) \approx 3 \times 10^{19}$ m^{-3} and central electron temperatures T_e between 2 and 4 keV were obtained in the experiments. Although

the central densities attained in the JET experiments are comparable to those expected in the initial phase of ITER, both the electron and the ion temperature were lower than those expected in the initial phase of ITER, which leads to a different collisional regime. In the experiments on ^{3}He heating by a second harmonic ^{3}He was injected into the hydrogen plasma. The injection of ^{3}He gas was controlled using a proportional-integral-derivative (PID) feedback control on the gas valve actuation based on real-time measurements of the line emission intensities for several ion species by means of the spectroscopy in the visible spectrum [14]. The ^{3}He concentration, defined as $X(^3\text{He}) = n(^3\text{He})/n_e$, was varied between 5 and 25% in these experiments. (It should be noted, however, that the concentration of ^{3}He in ITER is expected to be lower). To avoid ICRF power absorption or particle acceleration due to the residual ^{3}He in the plasma edge, the fundamental H majority heating experiments were performed first.

The VUV spectral range contains spectral lines from a wide range of elements and their various ionization states, making this range particularly valuable from the point of view of diagnosing high temperature plasmas. Spectroscopic measurements reported below were performed using Princeton Instruments survey SPRED [5] spectrometers, known on JET as KT2 [3] and KT7/2 [15] diagnostics. The KT2 diagnostic uses routinely a 450 g/mm holographic grating and measures VUV spectra in the 100–1100 Å wavelength range, with a spectral resolution of ~ 5 Å. It has a horizontal line of sight along the vessel mid-plane (see Fig. 1), allowing it to view the emission from the core and scrape-off layer of the plasma. The KT7/2 spectrometer has a 2105 g/mm grating and records spectra in the wavelength range of 140–440 Å. It looks nearly vertically down into the JET divertor (see Fig. 1). The detectors are micro-channel plates (MCP) and a phosphor screens. The radiation from phosphor is coupled by a fibre optic cable to a 2048 Photo Diode Array (PDA). The holographic grating of the SPRED spectrometer is designed to give a flat focal field, so that the spectral line profiles are very similar throughout the entire observed spectral region. Due to this fact the spectral line integration may be performed simply by applying Simpson's rule [1] to an area defined by a given number of pixels on either side of the line centre, these pixels also defining the background to be subtracted [8]. With 2048 pixels, an integration range covering ± 5 pixels from the line centre was regarded as the best compromise between minimizing blending and using a sufficient proportion of the line profile to ensure reliable results. In order to fully exploit the line intensity measurements, an absolute sensitivity calibration for KT2 and KT7/2 spectrometers was made. The relevant techniques are described in detail in [8] and [15], respectively.
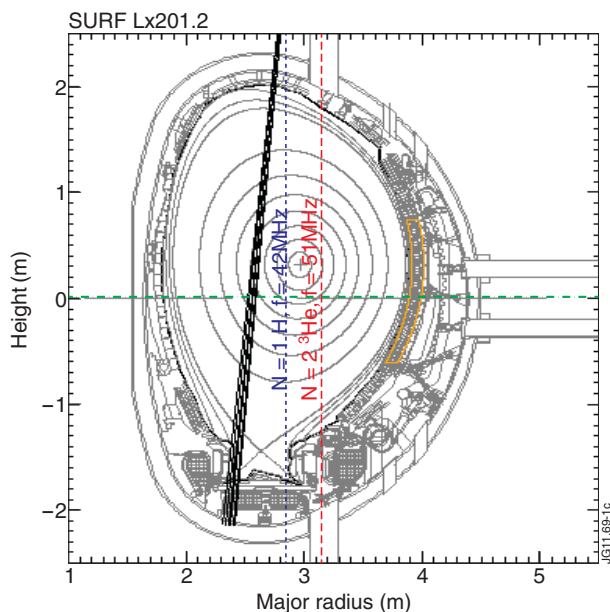

Fig. 1. The poloidal cross section of the JET vacuum vessel and the plasma profile. The lines of sight for the KT2 (–•–) and KT7 (—) diagnostics are shown, and the position of the resonance layers are indicated for the N = 1 H ($f = 42.5$ MHz) (∎∎∎) and N = 2 ^{3}He ($f = 51.5$ MHz) (---) heating scenarios.

Experimental results

Magnetically confined plasmas contain measurable amounts of impurity ions due to processes involving plasma-edge interactions with material surfaces. These include divertor plates, limiters, the vacuum vessel walls, and heating systems. To study the effect of fundamental

ICRF heating of H majority ions and second harmonic ICRF heating of ^{3}He ions on the plasma impurity content, the intensities of high ionization states of C-IV 312.40 Å and Ni-XXVI 165.04 Å were measured using the KT7 diagnostics. The measured intensity I of a particular line corresponding to the emission from the charge state $q+$ of the element with an atomic number Z can be expressed in a simple form

$$(1) \qquad\qquad I = n_Z^{q+} n_e F(T_e)$$

where n_e is the electron density and the function $F(T_e)$ takes into account the temperature dependence of all relevant atomic processes leading to the line emission. From the intensity of spectral lines in the light emitted by the impurity ions it is possible to calculate the number of photons that a population of ions with charge Z and a number density n_Z emits for a given transition at a local plasma electron temperature and density. From Eq. (1) it follows that for a fixed temperature the impurity concentration (expressed as the ratio of the impurity density n_z to the electron density n_e) is proportional to I/n_e^2. In a fusion device the temperature increases from the edge to the core and higher ionization states dominate in the plasma centre. In the JET plasmas, the low-Z elements such as C are fully ionized over most of the bulk plasma volume, and partially ionized charge states are concentrated at the plasma edge. Elements with moderate Z in the H-, He-, and Li-like ionization states may be found in the core. Since the C-IV ions are localized close to the plasma edge and the Ni-XXVI ions close to the plasma centre, the normalization of signals to the square of the local density becomes a reasonable measure of the impurity concentration in the plasma edge and core. To compare the impurity concentration in the plasma for both scenarios, discharges with nearly identical plasma conditions were selected. The VUV spectral line intensities of the high ionization states of Ni and C, normalized to the square of line integrated electron density (obtained from the LIDAR Thomson scattering diagnostics) are plotted in Fig. 2 as a function of the total ICRF power, for the N = 1 H and N = 2 ^{3}He heating modes. The data points in Fig. 2 were obtained by averaging over carefully selected time intervals of ~ 0.4 s duration with similar steady-state values of the electron density, temperature, NBI power (~ 1.3 MW) etc. in corresponding discharges. An important consequence of the low ICRF absorptivity of these scenarios [10] is the enhanced plasma-wall interaction leading to relatively large impurity content. We observed that the carbon and nickel concentrations for a given ICRF power are higher for the N = 2 ^{3}He case than for the fundamental H majority case. From Fig. 2 it can be seen that the concentration of impurities is ~ 2 times higher at 5 MW of P_{ICRH} for both C and Ni in N = 2 ^{3}He experiments. The same trend was observed for the effective charge of the plasma, Z_{eff} (see Fig. 3), derived from the bremsstrahlung emission by means of the spectroscopy in the visible spectrum [12] and the total radiated power obtained from bolometric measurements (see Fig. 4) as a function of the supplied ICRF power. This is related to a stronger RF-induced plasma-wall interaction observed for the N = 2 ^{3}He minority heating scheme leading to a higher impurity content in the plasma. The
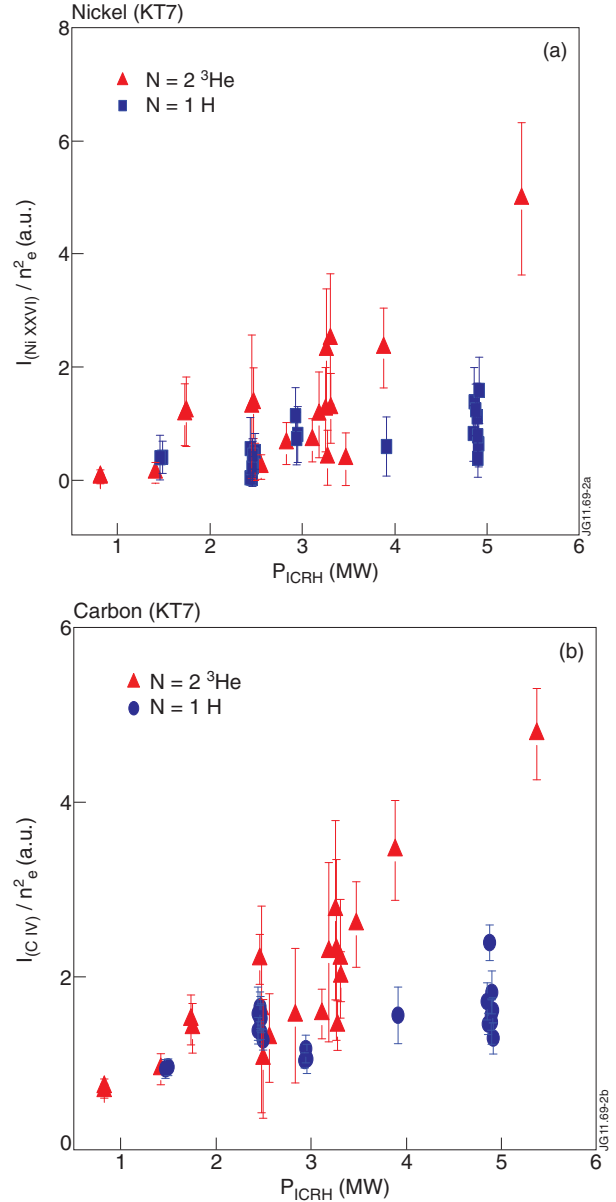

Fig. 2. The intensity of (a) the Ni-XXVI line and (b) the C-IV line, normalized to the square line integrated electron density (obtained from the LIDAR Thomson scattering diagnostics), as a function of the total ICRF power for the N = 1 H (circles) and the N = 2 ^{3}He (triangles) ICRF heating scenarios. The ratio I/n_e^2 is proportional to the impurity concentration. The data points correspond to a time average over a 0.4 s interval, averaged over discharges with similar densities, temperatures and NBI power.

origin of the RF-induced impurity generation is thought to be due to rectification of the RF waves, leading to the generation of the electric field by the antenna structure, which then causes acceleration of ions to energies high enough to cause a substantial sputtering of particles into the plasma and onto the antenna components. The fact that the impurity content is higher for N = 2 ^{3}He experiments despite similar ICRF heating efficiencies (and similar antenna coupling conditions) is believed to be related not only to different RF sheath rectification effects at the two distinct operation frequencies, but also to the enhanced fast ion losses observed in the two cases [10]. To obtain quantitative estimates for the
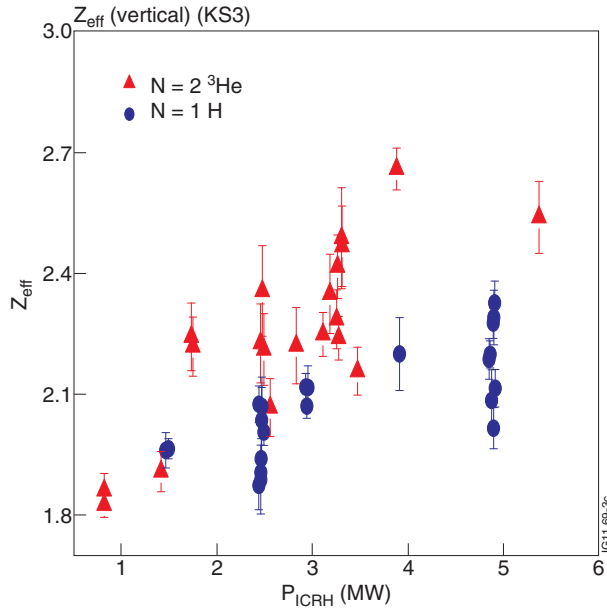
Fig. 3. The effective charge of the plasma, ΔZ_{eff}, as a function of the total ICRF power for the N = 1 H (circles) and the N = 2 ^{3}He (triangles) ICRF heating scenarios. The data points correspond to a time average over a 0.4 s time interval, averaged over discharges with similar densities, temperatures and NBI power.
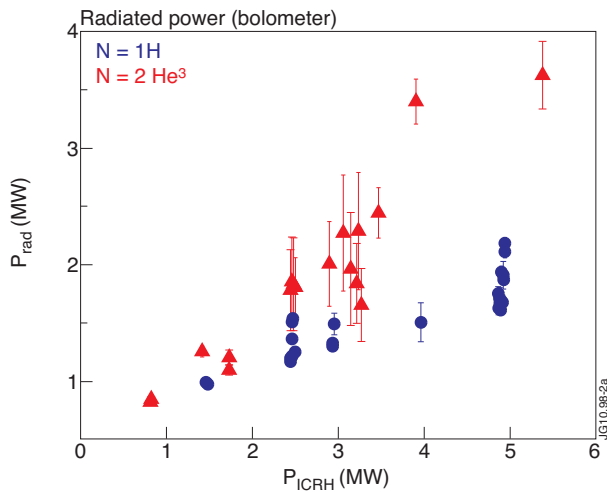

Fig. 4. The total radiated power as a function of the ICRF power for the N = 1 H (circles) and the N = 2 ^{3}He (triangles) ICRF heating scenarios. The data points correspond to a time average over a 0.4 s time interval, averaged over discharges with similar densities, temperatures and NBI power.

impurity content a complete description of the impurity behaviour must take into account the transport of ions across magnetic surfaces, which changes the ionization balance. Recently, a novel spectroscopic technique was established on JET for the determination of the metal impurity density, the ΔZ_{eff}, and the dilution, which account for the impact of the impurity transport and the electron temperature. This technique relies on the absolutely calibrated line intensities measured using the KT2 diagnostics, as well as simulations involving universal transport code (UTC), as described in [4]. The Ni impurity density n_z, the contribution of Ni to the effective charge of the plasma, ΔZ_{eff}, and the plasma dilution, Δn_{HDT}, Δn_{HDT} are given by [4]:

$$(2) \qquad n_z = (a_1 + b_1 \cdot T_e) \cdot \frac{I}{n_e} \ [m^{-3}]$$

$$(3) \qquad \Delta Z_{eff} = (a_2 + b_2 \cdot T_e) \cdot \frac{I}{n_e^2}$$

$$(4) \qquad \Delta n_{HDT} = (a_3 + b_3 \cdot T_e) \cdot \frac{I}{n_e} \ [m^{-3}]$$

where a_i and b_i ($i = 1, 2, 3$) are the coefficients of the linear fits in temperature of the derived quantities for the impurity, listed in [4], I (Ph·m^{-2}·s^{-1}·sr^{-1}) is the line intensity after taking into account the sensitivity calibration factor, T_e (keV) is the local electron temperature,
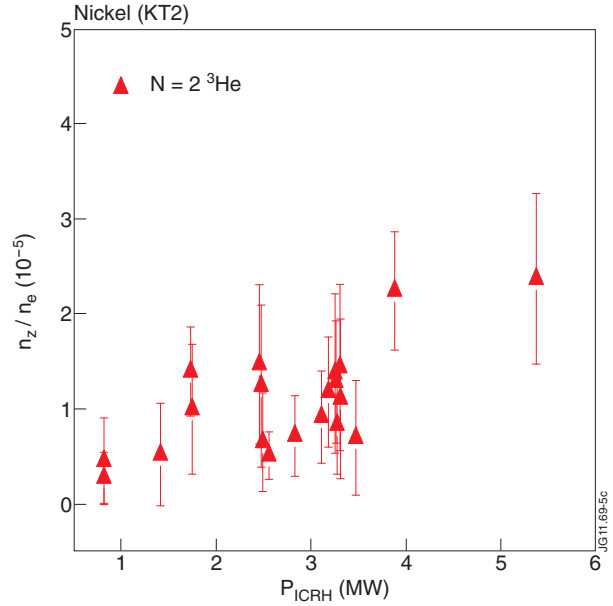

Fig. 5. The correlation between the Ni concentration ($r/a \approx$ 0.5–0.6) and the total applied heating power for N = 2 ^{3}He heating scenario. The data points correspond to a time average over a 0.4 s time interval, averaged over discharges with similar densities, temperatures and NBI power.
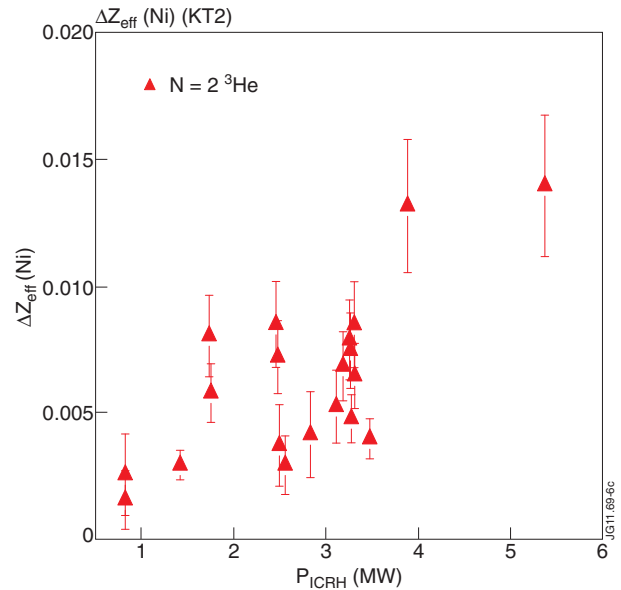

Fig. 6. The contribution of the Ni impurity to Z_{eff} ($r/a \approx$ 0.5–0.6), as a function of the total applied heating power. The data points correspond to a time average over a 0.4 s time interval, averaged over discharges with similar densities, temperatures and NBI power.

Plasma dilution (KT2)

Fig. 7. The plasma dilution due to the Ni impurity ($r/a \approx$ 0.5–0.6), as a function of the supplied ICRF power. The data points correspond to a time average over a 0.4 s time interval, averaged over discharges with similar densities, temperatures and NBI power.
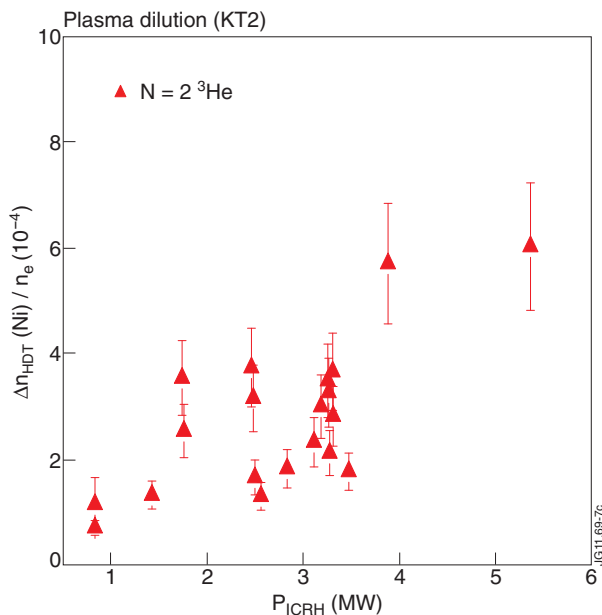
and n_e (m^{-3}) is the local electron density for the values of r/a between 0.5 and 0.6. The HDT subscript in Eq. (4) indicates hydrogen, deuterium and tritium plasma. A plot of the Ni concentration in mid-radius region obtained in this way is shown in Fig. 5 as a function of the applied ICRF heating power in JET. The contribution to Z_{eff} of the Ni impurity generated directly from the ICRH antenna is small. This can be seen in Fig. 6, where ΔZ_{eff}(Ni) is plotted vs. total ICRF heating power. The level of the plasma dilution due to the Ni impurity as a function of the total ICRF heating power during experiments with ^{3}He is presented in Fig. 7. Unfortunately, only the KT2 diagnostics was in operation during experiments with ^{3}He. However, since the estimates based on the ratio I/n_e^2 indicate reduced impurity content in both heating schemes, we would expect to obtain lower absolute values for impurity concentrations also in the N = 1 H heating scenario.

Conclusions

Experiments show that impurity concentration at JET with a C wall observed when the 2nd harmonic ^{3}He ICRF heating scenario was realized is higher than for the fundamental H majority heating scheme. There are several factors that may contribute to this behaviour: (i) the differences in the RF sheath rectification effects at the two different operation frequencies; (ii) the differences in the single pass absorption; and (iii) the differences in the fast ion populations impinging on the first wall. Because the ICRF antennas for ITER would have different structure than the ICRF antennas at JET, we can expect different rectified electric field on the antenna structures and thus different ion acceleration and sputtering of particles from the first wall components. In addition, one should keep in

mind that these experiments were done in JET with a C wall, while the wall on ITER would be Be+W and would generate different impurities. For this reason it is difficult to make precise quantitative conclusions for ITER. However, the results reported here suggest that the total ICRF power level in ITER's half-field scenario may be limited due to radiation issues related to a weak power absorption and an increased interaction of the RF waves with the wall. The experiments reported here will be complemented by a new series of experiments in JET with the newly installed ITER-like wall.

References

1. Atkinson KE (1989) An introduction to numerical analysis, 2nd ed. John Wiley & Sons, New York
2. Budny R, Berry L, Bilato R *et al.* (2010) Benchmarking ICRF simulations for ITER. In: Proc of the 23rd IAEA Fusion Energy Conf, 11–16 October 2010, Daejon, Republic of Korea, ITR/P1-29
3. Coffey IH, Barnsley R (2004) First tritium operation of ITER-prototype VUV spectroscopy on JET. Rev Sci Instrum 75:3737–3739
4. Czarnecka A, Rzadkiewicz J, Zastrow KD, Lawson KD, Coffey IH, O'Mullane MG (2011) Determination of metal impurity density, ΔZ_{eff} and dilution on JET by VUV emission spectroscopy. Plasma Phys Control Fusion 53:035009
5. Fonck RJ, Ramsey AT, Yelle RV (1982) Multichannel grazing-incidence spectrometer for plasma impurity diagnosis: SPRED. Appl Optics 21:2115–2123
6. Gormezano C, Sipps ACC, Luce TC *et al.* (2007) Steady state operation. Nucl Fusion 47:S285–S336
7. ITER Physics Basis Editors (1999) Chapter 1: Overview and summary. Nucl Fusion 39:2137–2174
8. Lawson KD, Coffey IH, Zacks J, Stamp MF (2009) An absolute sensitivity calibration of the JET VUV SPRED spectrometer. JINST 4 P04013
9. Lawson KD, Peacock NJ, Hawkes NC *et al.* (1987) Validation of KT2 data and the SAS, spectroscopic database. TAN 1/3
10. Lerche E, Van Eester D, Johnson T *et al.* (2010) Potential of the ICRF heating schemes foreseen for ITER's half--field hydrogen phase. In: Proc of the 23rd IAEA Fusion Energy Conf, 11–16 October 2010, Daejon, Republic of Korea, THW/P2-03
11. Lerche E, Van Eester D, Johnson T *et al.* (2011) Experimental investigation of ICRF heating scenarios for ITER's half-field hydrogen phase performed in JET. Plasma Phys Control Fusion 53:124019
12. Morgan PD, Behringer KH, Carolan PG, Forrest MJ, Peacock NJ, Stamp MF (1985) Spectroscopic measurements on the Joint European Torus using optical fibers to relay visible radiation. Rev Sci Instrum 56:862–864
13. Swain DW, Goulding R (2007) ITER ion cyclotron system: Overview and plans. Fusion Eng Design 82:603–609
14. Van Eester D, Lerche E, Andrew Y *et al.* (2009) JET (^{3}He)-D scenarios relying on RF heating: survey of selected recent experiments. Plasma Phys Control Fusion 51:044007

15. Zacks J (2008) Edge modelling of carbon impurities in JET plasmas. Ph D Thesis, Astrophysics Research Centre, School of Mathematics and Physics Queen's University Belfast, Belfast, Northern Ireland